Longer-range lattice anisotropy strongly competing with spin-orbit interactions in pyrochlore iridates

L. Hozoi,[1] H. Gretarsson,[2] J. P. Clancy,[2] B.-G. Jeon,[3] B. Lee,[3] K. H. Kim,[3] V. Yushankhai,[4,5] Peter Fulde,[4,6] D. Casa,[7] T. Gog,[7] Jungho Kim,[7] A. H. Said,[7] M. H. Upton,[7] Young-June Kim,[2] and Jeroen van den Brink[1,8]

[1]*Institute for Theoretical Solid State Physics, IFW Dresden, Helmholtzstr. 20, 01069 Dresden, Germany*
[2]*Department of Physics, University of Toronto, 60 St. George Street, Toronto, Ontario M5S 1A7, Canada*
[3]*CeNSCMR, Department of Physics and Astronomy, Seoul National University, Seoul 151-747, Korea*
[4]*Max-Planck-Institut für Physik komplexer Systeme, Nöthnitzer Str. 38, 01187 Dresden, Germany*
[5]*Joint Institute for Nuclear Research, Joliot-Curie 6, 141980 Dubna, Russia*
[6]*POSTECH, San 31 Hyoja-dong, Namgu Pohang, Gyeongbuk 790-784, Korea*
[7]*Advanced Photon Source, Argonne National Laboratory, Argonne, Illinois 60439, USA*
[8]*Department of Physics, Technical University Dresden, D-01062 Dresden, Germany*

(Received 31 October 2012; revised manuscript received 17 February 2014; published 11 March 2014)

In the search for topological phases in correlated electron systems, materials with 5*d* transition-metal ions, in particular the iridium-based pyrochlores $A_2Ir_2O_7$, provide fertile grounds. Several topological states have been predicted but the actual realization of such states is believed to critically depend on the strength of local potentials arising from distortions of the IrO_6 cages. We test this hypothesis by measuring with resonant inelastic x-ray scattering the electronic level splittings in the A = Y, Eu systems, which we show to agree very well with *ab initio* quantum chemistry electronic-structure calculations for the series of materials with A = Sm, Eu, Lu, and Y. We find, however, that the primary source for quenching the spin-orbit interaction is not a distortion of the IrO_6 octahedra but longer-range lattice anisotropies which inevitably break the local cubic symmetry.

DOI: 10.1103/PhysRevB.89.115111 PACS number(s): 71.27.+a, 03.65.Vf, 75.10.Jm, 78.70.Ck

I. INTRODUCTION

It is remarkable that the electronic bands of simple, noninteracting electron systems have intrinsic topological properties which have only recently been uncovered [1–3]. The presence of an insulating state of topological nature has been established in, for instance, a number of bismuth based materials [4–6], where this state is driven by the strong spin-orbit interaction (SOI) of the rather delocalized bismuth 6*p* electrons. These materials can be classified as either strong or weak topological insulators (TI's) [7–9].

The observed richness of topological states already on the single-electron level prompts the intriguing question: What kind of topological phases can develop in more strongly correlated, many-body electron systems? Correlation effects, in particular intra- and interorbital electron-electron interactions, are very substantial in 3*d* transition-metal compounds such as the copper oxides. However, they become progressively weaker when going to heavier transition-metal elements, i.e., 4*d* and 5*d* systems, as the *d* orbitals become more and more extended. Yet the relativistic SOI, the root cause of a number of many topologically nontrivial electronic states, follows the opposite trend—it increases progressively when going from 3*d* to 5*d* elements. In 5*d* transition-metal compounds like the iridates, the interesting situation arises that the SOI and Coulomb interactions meet on the same energy scale. The electronic structure of iridates therefore depends on a strong competition between the electronic hopping amplitudes, local energy-level splittings, electron-electron interaction strengths, and the SOI of the Ir 5*d* electrons. It is very interesting that the interplay of these ingredients in principle allows the stabilization of entirely novel electronic states such as strong or weak topological Mott states, an axion insulator or a Weyl semimetallic state [10–14].

In the pyrochlore iridates of the type $A_2Ir_2O_7$ that we consider here, with A = Sm, Eu, Lu, and Y, five electrons occupy the three Ir t_{2g} orbitals, which reside at Ir^{4+} sites inside corner-linked IrO_6 octahedra, see Fig. 1. This leaves one hole in the t_{2g} shell to which thus six distinct t_{2g} quantum states (three orbital and two spin) are available. When the local symmetry is cubic, so that it does not lift the degeneracy of the three t_{2g} levels, the strong SOI splits the t_{2g} states up into a pure $j = 3/2$ quadruplet and a pure $j = 1/2$ doublet. The doublet is higher in energy and therefore accommodates the hole. Any additional crystal-field splitting, for instance of tetragonal or trigonal symmetry, lifts the degeneracy of t_{2g} states and competes with the spin-orbit coupling, thus tending to quench the orbital moment. As the SOI is driving the formation of electronic states of topological nature, the outcome of this competition is decisive for the actual realization of any type of nontrivial topological ground state in pyrochlore iridates [15,16].

II. EXPERIMENTAL RIXS RESULTS

We use resonant inelastic x-ray scattering (RIXS) [17] to measure directly the energy of the different configurations of a hole in the Ir t_{2g} shell [18] of $Y_2Ir_2O_7$ and $Eu_2Ir_2O_7$ and to determine in that way the crystal-field energy splittings of these states. The single crystals of $Eu_2Ir_2O_7$ and powder samples of $Y_2Ir_2O_7$ were grown by solid-state synthesis. Mixtures of Y_2O_3 and IrO_2 with purities of 99.99% were ground in stoichiometric molar ratios, pelletized, and then heated in air at 1000 °C for 100 hours. The resulting material was reground, pressed into pellets, and resintered at the same temperature for an additional 150 hours, with two intermediate regrindings. Powder x-ray diffraction measurements confirmed the phase purity of the resulting $Y_2Ir_2O_7$ sample to within the resolution

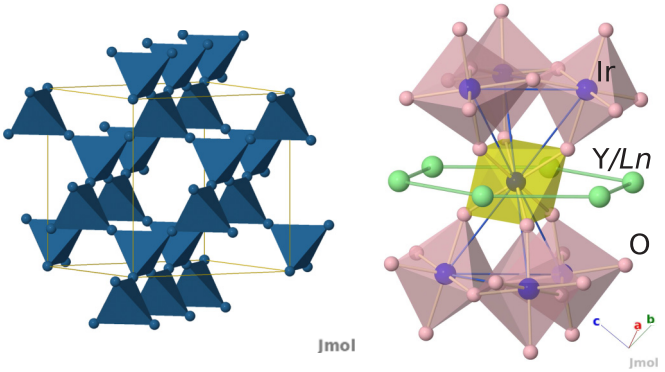

FIG. 1. (Color online) (a) Network of corner-linked Ir_4 tetrahedra in $A_2Ir_2O_7$ pyrochlore iridates. (b) A central IrO_6 octahedron and how it is connected to its six neighboring IrO_6 octahedra. The six trivalent A-site atoms form a hexagonal ring around the central octahedron.

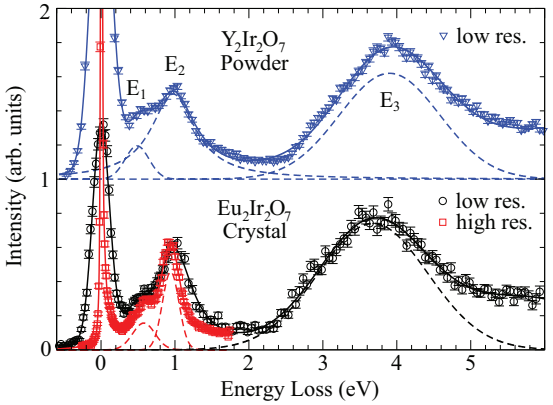

FIG. 2. (Color online) Resonant inelastic x-ray scattering spectra of $Y_2Ir_2O_7$ (top) and $Eu_2Ir_2O_7$ (bottom) at the iridium L edge. The $Eu_2Ir_2O_7$ spectra were collected at $\mathbf{Q} = (8.45,8.45,7)$. For $Eu_2Ir_2O_7$, high resolution data obtained for the low energy region at (7.8,7.8,7.8) are also plotted to emphasize the intrinsic nature of the peak width. Dashed curves are the result of fitting (see text).

of the measurement. A single crystal of $Eu_2Ir_2O_7$ was grown by the solid-state synthesis method, as previously described in detail in Ref. [19]. A mixture of polycrystalline $Eu_2Ir_2O_7$ and KF (2N) were heated up to 1100 °C and next cooled down to 850 °C at a rate of 2.5°/h. Resistivity data on the resulting $Eu_2Ir_2O_7$ single crystal shows almost metallic behavior, indicating that the sample displays slight excess of Ir, see the discussion in Ref. [20].

RIXS is a second-order scattering technique and can directly probe the electronic transitions within the Ir $5d$ manifold due to two successive electric dipole transitions ($2p \rightarrow 5d$ followed by $5d \rightarrow 2p$) [17,18]. It is therefore a valuable technique for detecting transitions between crystal-field split Ir $5d$ levels and has been utilized for a variety of iridates [21–25]. We determine the splittings by measuring the d-d transition energies at the iridium L_3 edge, with an incident energy, $E_i = 11.217$ keV, chosen to maximize the resonant enhancement of the spectral features of interest below 1.5 eV. It should be noted that varying the incident energy did not result in a shift of any of the peaks but merely changed their intensities, a behavior associated with valence excitations [21–25]. The experiments were carried out at the Advanced Photon Source using the 9ID beamline with a Si(444) channel-cut secondary monochromator and a horizontal scattering geometry. A spherical (1 m radius) diced Si(844) analyzer was used and an overall energy resolution of 175 meV (FWHM) was obtained. Higher resolution measurements were carried out using the MERIX spectrometer on beamline 30-ID-B. Measurements were performed using a spherical (2 m radius) diced Si(844) analyzer and a channel-cut Si(844) secondary monochromator to give an overall energy resolution (FWHM) of 35 meV.

Due to experimental conditions, the spectra for $Y_2Ir_2O_7$ and $Eu_2Ir_2O_7$ were obtained at two different temperatures, 300 and 150 K, respectively. Since the thermal contraction of $Y_2Ir_2O_7$ is extremely small, within tenths of a percentage between 300 and 150 K, and the local oxygen octahedra are unaffected by the temperature [26], we can conclude that this difference in temperature has minimum bearing on our results. The RIXS spectra of both $Y_2Ir_2O_7$ and $Eu_2Ir_2O_7$ in Fig. 2 show sharp features below 1.5 eV, corresponding to transitions within the Ir t_{2g} levels, and a strong intense peak stretching from 2 to 5 eV that according to the calculations, see below, corresponds to d-d transitions between the Ir t_{2g} and e_g levels. To quantitatively analyze the RIXS spectra, the various peaks were fitted with analytical functions, as shown by the dashed lines in Fig. 2. The low-energy excitations, E_1 and E_2, were fitted with one Gaussian and one Lorentzian, respectively. The Lorentzian function was used in order to capture some of the tail on the high energy side (∼1.5 eV). The high-energy excitations (E_3) were fitted with a Gaussian peak on top of a sloping background. Such a sloping background may come from charge transfer excitations which are expected to appear in this range.

The position refinement for the three main peaks apart from the zero-loss peak results in $E_1 = 0.53 \pm 0.05$ (0.59 ± 0.03), $E_2 = 0.98 \pm 0.05$ (0.97 ± 0.03), and $E_3 = 3.90 \pm 0.05$ eV (3.70 ± 0.05 eV) for $Y_2Ir_2O_7$ ($Eu_2Ir_2O_7$). Note that the peak widths are significantly broader than the instrumental resolution, which is about 175 meV. To check this, we carried out an additional measurement on the same $Eu_2Ir_2O_7$ sample employing much higher energy resolution of 35 meV. This high resolution spectrum is overlayed on top of the low resolution data in Fig. 2. As expected, the improved resolution reveals a little bit sharper features, but still with intrinsic spectral width of about 300 meV. We note that the fitted E_2 peak position of the high resolution data, 0.95 ± 0.01 eV, is slightly smaller than that of the low resolution data, but still within the experimental error bar. Since the high resolution result has a smaller error bar, this value is quoted in Table I. We also observed no noticeable momentum dependence for $Eu_2Ir_2O_7$, justifying the use of $Y_2Ir_2O_7$ powder samples for our comparison.

III. EMPIRICAL DESCRIPTION OF RIXS RESULTS

Using a first, empirical ansatz we fit the energies of the low-lying E_1 and E_2 peaks to the eigenvalues of an effective single-ion Hamiltonian for the t_{2g} orbitals of the form

TABLE I. Relative energies (in eV) of the split $j=3/2$ states E_1 and E_2 as well as t_{2g}^5 to $t_{2g}^4 e_g^1$ excitation energies in 227 iridates. The results are the outcome of *ab initio* spin-orbit MRCI calculations, see text. The experimental values for $Eu_2Ir_2O_7$ and $Y_2Ir_2O_7$ determined from their RIXS spectra in Fig. 2 are shown in bold, within brackets.

	E_1	E_2	$t_{2g}^4 e_g^1$
$Sm_2Ir_2O_7$	0.61	0.91	3.41–4.75
$Eu_2Ir_2O_7$	0.60 (**0.59**)	0.91 (**0.95**)	3.39–4.72 (**3.70**)
$Lu_2Ir_2O_7$	0.57	0.92	3.49–4.88
$Y_2Ir_2O_7$	0.58 (**0.53**)	0.94 (**0.98**)	3.48–4.84 (**3.90**)

$H_0=\lambda \boldsymbol{l}\cdot\boldsymbol{s}-\Delta l_z^2$, where λ is the SOI strength and Δ the t_{2g} crystal-field splitting [24,27,28]. The latter tends to quench the Ir orbital moment and is usually identified with distortions of the IrO_6 octahedra [15,29]. The eigenvalues of H_0 and the splittings among the spin-orbit t_{2g}^5 states are given by the following expressions: $E_0=\lambda(-1+\delta-\sqrt{9+2\delta+\delta^2})/4$, $E_1=\lambda/2$, and $E_2=\lambda(-1+\delta+\sqrt{9+2\delta+\delta^2})/4$, where E_0 is the energy of the ground-state spin-orbit $j=1/2$ doublet, E_1 and E_2 define the eigenvalues of the split $j=3/2$ -like terms, and $\delta=2\Delta/\lambda$. If E_1-E_0 and E_2-E_0 are known from experiment, i.e., RIXS, simple estimates for λ and Δ can be in principle derived from the relations above. In particular, $\lambda=2(2E_{10}-E_{20})/(3-\delta)$ and $\Delta=\lambda\delta/2$, where $\delta=-b-\sqrt{b^2-9}$, $b=(1+3a^2)/(1-a^2)$, $a=E_{20}/(E_{20}-2E_{10})$, $E_{20}=E_2-E_0$, and $E_{10}=E_1-E_0$. The fit of the RIXS data to such a λ–Δ model yields the effective parameters $\lambda=0.43$ and $\Delta=0.56$ eV for Y-227 and $\lambda=0.46$ and $\Delta=0.46$ eV for Eu-227. The value of λ for each of these materials agrees with values of 0.39–0.49 eV extracted from electron spin resonance measurements on Ir^{4+} impurities [30]. The magnitude of Δ, 0.46–0.56 eV, however, is surprisingly large. To understand the size and elucidate the microscopic origin of this large crystal-field splitting—a crucial energy scale in determining the topological ground state of the electronic system—we have carried out a set of detailed *ab initio* calculations of the Ir d-level electronic structure on a series of $5d^5$ pyrochlore iridates: Sm-, Eu-, Lu-, and Y-227.

IV. *AB INITIO* CALCULATION OF D-D EXCITATIONS

To investigate in detail the electronic structure and the essential interactions in the $A_2Ir_2O_7$ iridates, we rely on *ab initio* many-body techniques from wave-function-based quantum chemistry [31]. Multiconfiguration self-consistent-field (MCSCF) and multireference configuration-interaction (MRCI) calculations [31] were carried out to this end on properly embedded finite clusters. Since it is important to accurately describe the charge distribution at sites in the immediate neighborhood [32–34], we explicitly include in the actual cluster the closest six A-ion neighbors and the six adjacent IrO_6 octahedra around the reference IrO_6 unit for which the Ir d-d excitations are explicitly computed, see also Refs. [24,25,35–37]. The solid-state surroundings were further modeled as a large array of point charges fitted to reproduce the crystal Madelung field in the cluster region. All calculations were performed with the MOLPRO quantum chemistry software [38].

TABLE II. Calculated energies, E_1^0, E_2^0, of the $j=3/2$ -like spin-orbit states in idealized crystal structures without trigonal distortion of the IrO_6 octahedra. Those states are split even without trigonal squashing. $\bar{\Delta}^0$ and $\bar{\Delta}$ are the splitting of the Ir t_{2g} levels in MRCI calculations without SOI in the undistorted idealized and experimental (Ref. [45]) crystal structures, respectively.

	Undistorted Octahedron		Without SOI	
	E_1^0	E_2^0	$\bar{\Delta}^0$	$\bar{\Delta}$
$Eu_2Ir_2O_7$	0.67	0.89	0.30	0.27
$Y_2Ir_2O_7$	0.66	0.90	0.32	0.30

We used energy-consistent relativistic pseudopotentials for Ir and the A elements [39–42] and Gaussian-type valence basis functions. Basis sets of quadruple-zeta quality were applied for the valence shells of the central Ir^{4+} ions [39] and triple-zeta basis sets for the ligands [43] of the central octahedron and for the nearest-neighbor (NN) Ir sites [39]. For the central Ir ions we also used two polarization f functions [39]. For farther O's around the NN Ir sites we applied minimal atomic-natural-orbital basis sets [44]. The f electrons of the Ln^{3+} species were incorporated in the effective core potentials [40,41] and the outer sp shells of the Ln^{3+} and Y^{3+} ions were modeled with sets of $[3s2p]$ functions [40–42]. Crystallographic data as reported by Taira *et al.* [45] were employed.

For the ground-state calculations, the orbitals within each finite cluster are variationally optimized at the MCSCF level. All Ir t_{2g} functions are included in the active orbital space [31], i.e., all possible electron occupations are allowed within the t_{2g} set of orbitals. On-site t_{2g} and t_{2g} to e_g excitations are afterwards computed just for the central IrO_6 octahedron while the occupation of the NN Ir valence shells is held frozen as in the ground-state configuration. The MRCI treatment includes on top of the MCSCF wave functions single and double excitations [31] from the O $2p$ orbitals at the central octahedron and the Ir $5d$ orbitals.

To extract the local Ir t_{2g} splittings, the NN Ir^{4+} d^5 ions were explicitly included in a first set of MCSCF calculations. However, the presence of six open-shell Ir NN's makes the spin-orbit calculations cumbersome because for seven $5d^5$ sites (and nondegenerate orbitals), a given electron configuration implies 1 octet, 6 sextet, 14 quartet, and 14 doublet states which further interact via spin-orbit coupling. To simplify the problem and reduce the computational effort, we therefore further replaced the six Ir^{4+} d^5 NN's by closed-shell Pt^{4+} d^6 ions[1] and in this manner obtained the relative MRCI energies for the spin-orbit states presented in Tables I and II.

The d-d splittings calculated for cuprates such as La_2CuO_4 and Sr_2CuO_3 [33,46,47] and iridates such as Sr_2IrO_4, Na_2IrO_3, and Sr_3CuIrO_6 [24,25,35] by similar quantum chemistry techniques are in close agreement to the experimental values of these excitation energies. Also for the 227 iridium pyrochlores that we consider here, we observe that the calculated excitation

[1]This is an usual procedure in quantum chemistry studies on transition-metal systems, see, e.g., Refs. [32,37,55,56].

energies of the $5d$ multiplets (the values of E_1, E_2, and E_3), see Table I, are in close agreement with the ones obtained from our RIXS experiments.

V. DISCUSSION

The good agreement between calculated and measured d-d excitation energies forms the basis for a subsequent detailed analysis of the microscopic origin of the crystal-field splitting of the Ir $5d$ levels. To this end, we first test the hypothesis that the splitting Δ in the effective single ion $\lambda-\Delta$ model is due to a distortion of the IrO_6 octahedra which lowers the local cubic symmetry to trigonal (or even lower) symmetry. It turns out that the crystal structure of the 227's under consideration is fully defined by just three parameters: the space-group number, the cubic lattice constant a, and the fractional coordinate x of the O at the 48f site [45]. For $x=x_c=5/16$, the oxygen cage around each Ir site forms an undistorted, regular octahedron. In our 227 Ir pyrochlores, however, x is always larger than x_c, which translates into a compressive trigonal distortion of the IrO_6 octahedra and hence a splitting of the $5d$ electronic levels. To estimate how large the resulting trigonal crystal-field splitting is, we have performed a set of further *ab initio* calculations, but now for an idealized crystal structure with $x=x_c$ and thus undistorted octahedra. The results of the spin-orbit calculations listed in Table II show that the $j=3/2$ -like states are split off by a sizable amount even for $x=x_c$. Thus local trigonal distortions of the IrO_6 octahedra are *not* the main cause of the energy splitting Δ of the Ir t_{2g} levels.

To understand the physical origin of the large Ir t_{2g} splittings one needs to consider the crystal structure of the A-227's in more detail. As shown in Fig. 1(b), the A ions closest to a given Ir site form a hexagonal structure in a plane parallel to two of the facets of the IrO_6 octahedron. Even without pushing those two facets of the octahedral cage closer to each other, the six adjacent A cations generate a trigonal field that breaks cubic symmetry. In the simplest picture this positive potential stabilizes the Ir e_g' orbitals. The latter have the electronic charge closer to the plane defined by the six A NN's, as compared to the a_{1g} orbital. There is however a competing effect related to the positive NN Ir ions, three above and three below the plane of adjacent A sites, see Fig. 1. The potential generated by the Ir NN's stabilizes the a_{1g} sublevel. The numerical results we obtain, see below, indicate that the net effect of this anisotropic arrangement of the nearby A and Ir cations on the t_{2g} level splitting is stronger than the effect of the trigonal distortion of the IrO_6 cages. It is interesting to note that similar effects are expected in pyrochlore systems with $3d$ transition-metal ions. However, the $3d$ orbitals being more localized will reduce the effect of such anisotropies beyond the first ligand coordination shell and result in smaller splittings of the energy levels.

MRCI calculations without SOI's, see Table II, show that the magnitude of the t_{2g} splittings is about the same in the distorted, experimental crystal structure ($\bar{\Delta}$, $x>x_c$) and the idealized, undistorted structural model ($\bar{\Delta}^0$, $x=x_c$). This confirms that the splitting of the Ir t_{2g} levels is due to anisotropic potentials beyond the NN ligand coordination shell. The role of nearby cations in generating anisotropic fields that compete with the trigonal distortion of the ligand cage has been pointed out as early as the 60's for the spinel structure [48,49], recently confirmed by *ab initio* quantum chemistry calculations on the $S=3/2$ 227 pyrochlore $Cd_2Os_2O_7$ [37], and also analyzed for layered Co oxide compounds by density-functional calculations [50].

The calculations on the 227 iridates also show that the a_{1g} sublevel is lower in energy than the e_g' sublevels, which is usually referred to as negative trigonal splitting [50,51]. This indicates that the effect of the positive potential related to the six Ir NN's is stronger than the effect of the field generated by the closest A ions. A stabilization of the a_{1g} orbital due to positive ions on the trigonal axis has been earlier evidenced by Pillay *et al.* in Na_xCoO_2 [50]. Importantly, if in the quantum chemistry calculations the nuclear charge is artificially lowered by 1 at each of the six Ir NN sites and raised by 1 at each of the six A NN sites, the trigonal splitting changes sign.

While the *ab initio* calculations without SOI yield Δ values of $\approx$0.30 eV, the fit of the RIXS data with the effective $\lambda-\Delta$ model provides t_{2g} splittings Δ of 0.46–0.56 eV, more than 50% larger. This indicates that in pyrochlore iridates the effect of the relativistic spin-orbit coupling cannot be completely captured by oversimplified models such as the $\lambda-\Delta$ Hamiltonian. Additional degrees of freedom must be considered for the construction of a minimal effective model, i.e., hybridization effects, Ir–O and Ir e_g'–e_g, in the presence of trigonal external fields and also many-body d-shell correlations. The e_g'–e_g couplings, for instance, were found to be important in trigonally distorted $3d^5$ compounds [52]. Our data in Table II, showing that with trigonal distortions the a_{1g}–e_g' splittings decrease (as $\bar{\Delta}<\bar{\Delta}^0$), qualitatively confirm the quantum chemistry results of Landron and Lepetit [52], i.e., in the presence of trigonal squashing the e_g' levels are energetically favored as compared to the a_{1g} states, in contrast to naive expectations based on one-electron crystal-field theory. Obviously, for $5d$ oxides, the t_{2g}–e_g couplings are further enhanced by the strong SOI's [28,53].

It is also interesting that without trigonal distortions the lower doublet state originating from the $j=3/2$ quartet significantly shifts to higher energy as compared to the trigonally compressed experimental structure ($E_1<E_1^0$, see Tables I and II), although the splitting of the t_{2g} levels is about the same in the two cases. The other doublet at somewhat higher energy is on the other hand not much affected. A relevant detail is here that the Ir-O bond lengths are slightly reduced for the data in Table II because the lattice constant was kept the same and in order to remove the trigonal distortion only the fractional coordinate x of the O site was modified. Shorter Ir-O bonds yield higher electron density at the Ir site. The $5d$-shell Mulliken population [31], for instance, is larger by 0.1 of an electronic charge for the structural model without trigonal distortions. The results of the spin-orbit calculations in Tables I and II, with a sizable shift of the E_1^0 level to higher energy, indicate that the charge redistribution within the IrO_6 octahedron and the higher electron density at the Ir site effectively modify the spin-orbit couplings within the IrO_6 unit. Feeding the E_1^0 and E_2^0 quantum chemistry results of Table II to a simple λ–Δ model yields indeed a rather large λ effective parameter of 0.49–0.50 while the corresponding Δ's perfectly match this time the *ab initio* trigonal splittings $\bar{\Delta}^0$ computed with no trigonal distortions, 0.30 and 0.32 eV.

Thus in an idealized system, without trigonal distortions, the effective λ–Δ model provides a reasonable description. It is, however, clear that additional ingredients are required in the effective model for a qualitative description of, e.g., how those excitation energies evolve with the amount of trigonal distortion. This will be the topic of future investigations.

VI. CONCLUSIONS

We have presented here both experimental and theoretical evidence for the presence of large Ir t_{2g} splittings in pyrochlore iridates. These splittings arise from longer-range crystal anisotropies that directly compete with spin-orbit interactions. The canonical view that only local distortions of IrO_6 octahedra tend to quench the spin-orbit coupling in iridium compounds, in particular iridium pyrochlores, is therefore incomplete. The broader ramification is that the rather extended nature of the 5*d* wave functions renders the longer-range anisotropy fields to be of fundamental importance throughout the 5*d* transition-metal series. Their physical effect is particularly striking when the local ligand-field symmetry is high, e.g., cubic or close to cubic, but the point-group symmetry in the crystal is lower. This includes, for example, the osmium-based pyrochlore materials [37,54]. Yet it is pertinent for many more crystal structures, in particular for layered quasi-2D perovskites or chainlike quasi-1D 5*d* transition-metal systems [24,36].

ACKNOWLEDGMENTS

We thank N. A. Bogdanov, V. M. Katukuri, and H. Stoll for fruitful discussions. Research at the University of Toronto was supported by the NSERC, CFI, and OMRI. Use of the Advanced Photon Source at Argonne National Laboratory was supported by the U.S. Department of Energy under Contract No. DE-AC02-06CH11357. Work at SNU was supported by the National CRI (2010-0018300) program. L.H. acknowledges financial support from the German Research Foundation (Deutsche Forschungsgemeinschaft, DFG).

[1] C. Kane and E. Mele, Phys. Rev. Lett. **95**, 146802 (2005).
[2] B. A. Bernevig, T. L. Hughes, and S.-C. Zhang, Science **314**, 1757 (2006).
[3] M. König, S. Wiedmann, C. Brüne, A. Roth, H. Buhmann, L. W. Molenkamp, X.-L. Qi, and S.-C. Zhang, Science **318**, 766 (2007).
[4] D. Hsieh, D. Qian, L. Wray, Y. Xia, Y. S. Hor, R. J. Cava, and M. Z. Hasan, Nature (London) **452**, 970 (2008).
[5] H. Zhang, C.-X. Liu, X.-L. Qi, X. Dai, Z. Fang, and S.-C. Zhang, Nat. Phys. **5**, 438 (2009).
[6] B. Rasche, A. Isaeva, M. Ruck, S. Borisenko, V. Zabolotnyy, B. Buechner, K. Koepernik, C. Ortix, M. Richter, and J. van den Brink, Nat. Mater. **12**, 422 (2013).
[7] J. E. Moore and L. Balents, Phys. Rev. B **75**, 121306 (2007).
[8] L. Fu, C. L. Kane, and E. J. Mele, Phys. Rev. Lett. **98**, 106803 (2007).
[9] R. Roy, Phys. Rev. B **79**, 195322 (2009).
[10] H.-M. Guo and M. Franz, Phys. Rev. Lett. **103**, 206805 (2009).
[11] D. Pesin and L. Balents, Nat. Phys. **6**, 376 (2010).
[12] X. Wan, A. M. Turner, A. Vishwanath, and S. Y. Savrasov, Phys. Rev. B **83**, 205101 (2011).
[13] L. Balents, Physics **4**, 36 (2011).
[14] W. Witczak-Krempa and Y.-B. Kim, Phys. Rev. B **85**, 045124 (2012).
[15] B.-J. Yang and Y. B. Kim, Phys. Rev. B **82**, 085111 (2010).
[16] M. Kargarian, J. Wen, and G. A. Fiete, Phys. Rev. B **83**, 165112 (2011).
[17] L. J. P. Ament, M. van Veenendaal, T. P. Devereaux, J. P. Hill, and J. van den Brink, Rev. Mod. Phys. **83**, 705 (2011).
[18] L. J. P. Ament, G. Khaliullin, and J. van den Brink, Phys. Rev. B **84**, 020403 (2011).
[19] J. N. Millican, Mater. Res. Bull. **42**, 928 (2007).
[20] J. J. Ishikawa, E. C. T. O'Farrell, and S. Nakatsuji, Phys. Rev. B **85**, 245109 (2012).
[21] J. Kim, D. Casa, M. H. Upton, T. Gog, Y.-J. Kim, J. F. Mitchell, M. van Veenendaal, M. Daghofer, J. van den Brink, G. Khaliullin, and B. J. Kim, Phys. Rev. Lett. **108**, 177003 (2012).
[22] H. Gretarsson, J. Kim, D. Casa, T. Gog, K. R. Choi, S. W. Cheong, and Y.-J. Kim, Phys. Rev. B **84**, 125135 (2011).
[23] K. Ishii, I. Jarrige, M. Yoshida, K. Ikeuchi, J. Mizuki, K. Ohashi, T. Takayama, J. Matsuno, and H. Takagi, Phys. Rev. B **83**, 115121 (2011).
[24] X. Liu, V. M. Katukuri, L. Hozoi, W.-G. Yin, M. P. M. Dean, M. H. Upton, J. Kim, D. Casa, A. Said, T. Gog, T. F. Qi, G. Cao, A. M. Tsvelik, J. van den Brink, and J. P. Hill, Phys. Rev. Lett. **109**, 157401 (2012).
[25] H. Gretarsson, J. P. Clancy, X. Liu, J. P. Hill, E. Bozin, Y. Singh, S. Manni, P. Gegenwart, J. Kim, A. H. Said, D. Casa, T. Gog, M. H. Upton, H.-S. Kim, J. Yu, V. M. Katukuri, L. Hozoi, J. van den Brink, and Y.-J. Kim, Phys. Rev. Lett. **110**, 076402 (2013).
[26] S. Zhao, J. M. Mackie, D. E. MacLaughlin, O. O. Bernal, J. J. Ishikawa, Y. Ohta, and S. Nakatsuji, Phys. Rev. B **83**, 180402 (2011).
[27] A. Abragam and B. Bleaney, *Electron Paramagnetic Resonance of Transition Ions* (Clarendon Press, Oxford, 1970).
[28] J. H. M. Thornley, J. Phys. C (Proc. Phys. Soc.) **1**, 1024 (1968).
[29] G. Jackeli and G. Khaliullin, Phys. Rev. Lett. **102**, 017205 (2009).
[30] B. Andlauer, J. Schneider, and W. Tolksdorf, Phys. Status Solidi B **73**, 533 (1976).
[31] T. Helgaker, P. Jørgensen, and J. Olsen, *Molecular Electronic-Structure Theory* (Wiley, Chichester, 2000).
[32] C. de Graaf, C. Sousa, and R. Broer, J. Mol. Struct. (Theochem) **458**, 53 (1998).
[33] L. Hozoi, L. Siurakshina, P. Fulde, and J. van den Brink, Sci. Rep. **1**, 65 (2011).
[34] L. Hozoi and M. S. Laad, Phys. Rev. Lett. **99**, 256404 (2007).
[35] V. M. Katukuri, H. Stoll, J. van den Brink, and L. Hozoi, Phys. Rev. B **85**, 220402 (2012).
[36] N. A. Bogdanov, V. M. Katukuri, H. Stoll, J. van den Brink, and L. Hozoi, Phys. Rev. B **85**, 235147 (2012).
[37] N. A. Bogdanov, R. Maurice, I. Rousochatzakis, J. van den Brink, and L. Hozoi, Phys. Rev. Lett. **110**, 127206 (2013).

[38] H.-J. Werner, P. J. Knowles, G. Knizia, F. R. Manby, and M. Schütz, MOLPRO 2010, see http://www.molpro.net.
[39] D. Figgen, K. A. Peterson, M. Dolg, and H. Stoll, J. Chem. Phys. **130**, 164108 (2009).
[40] M. Dolg, H. Stoll, A. Savin, and H. Preuss, Theor. Chim. Acta **75**, 173 (1989).
[41] M. Dolg, H. Stoll, A. Savin, and H. Preuss, Theor. Chim. Acta **85**, 441 (1993).
[42] K. A. Peterson, D. Figgen, M. Dolg, and H. Stoll, J. Chem. Phys. **126**, 124101 (2007).
[43] T. H. J. Dunning, J. Chem. Phys. **90**, 1007 (1989).
[44] K. Pierloot, B. Dumez, P.-O. Widmark, and B. O. Roos, Theor. Chim. Acta **90**, 87 (1995).
[45] N. Taira, M. Wakeshima, and Y. Hinatsu, J. Phys.: Condens. Matter **13**, 5527 (2001).
[46] J. Schlappa, K. Wohlfeld, K. J. Zhou, M. Mourigal, M. W. Haverkort, V. N. Strocov, L. Hozoi, C. Monney, S. Nishimoto, S. Singh, A. Revcolevschi, J.-S. Caux, L. Patthey, H. M. Rønnow, J. van den Brink, and T. Schmitt, Nature (London) **485**, 82 (2012).
[47] H.-Y. Huang, N. A. Bogdanov, L. Siurakshina, P. Fulde, J. van den Brink, and L. Hozoi, Phys. Rev. B **84**, 235125 (2011).
[48] J. C. Slonczewski, J. Appl. Phys. **32**, S253 (1961).
[49] S. B. Berger, J. Appl. Phys. **36**, 1048 (1965).
[50] D. Pillay, M. D. Johannes, I. I. Mazin, and O. K. Andersen, Phys. Rev. B **78**, 012501 (2008).
[51] S. Sugano and Y. Tanabe, J. Phys. Soc. Jpn. **13**, 880 (1958).
[52] S. Landron and M.-B. Lepetit, Phys. Rev. B **77**, 125106 (2008).
[53] D. Haskel, G. Fabbris, M. Zhernenkov, P. P. Kong, C. Jin, G. Cao, and M. van Veenendaal, Phys. Rev. Lett. **109**, 027204 (2012).
[54] H. Shinaoka, T. Miyake, and S. Ishibashi, Phys. Rev. Lett. **108**, 247204 (2012).
[55] L. Hozoi, A. H. de Vries, A. B. van Oosten, R. Broer, J. Cabrero, and C. de Graaf, Phys. Rev. Lett. **89**, 076407 (2002).
[56] R. Maurice, P. Verma, J. M. Zadrozny, S. Luo, J. Borycz, J. R. Long, D. G. Truhlar, and L. Gagliardi, Inorg. Chem. **52**, 9379 (2013).